ELSEVIER

Thermochimica Acta 392–393 (2002) 303–313

thermochimica acta

www.elsevier.com/locate/tca

Dynamics of reversible melting revealed from frequency dependent heat capacity

Christoph Schick*, Andreas Wurm, Alaa Mohamed

Department of Physics, University of Rostock, 18051 Rostock, Germany

Received 19 January 2001; accepted 4 May 2001

Abstract

Heat capacity of semi-crystalline polymers shows frequency dependence not only in the glass transition range. Also above glass transition and below melting temperature a frequency dependent heat capacity can be observed. The asymptotic value of heat capacity at high frequencies equals base-line heat capacity while the asymptotic value at low frequencies yield information about reversing melting. For polycarbonate (PC), poly(3-hydroxybutyrate) (PHB) and syndiotactic polypropylene (sPP) the asymptotic value at high frequencies can be measured by temperature-modulated DSC (TMDSC). For polycaprolactone (PCL) and sPP the frequency dependence of heat capacity can be studied in quasi-isothermal TMDSC experiments. The heat capacity spectra were obtained from single measurements applying multi-frequency perturbations (spikes in heating rate) like in StepScan™ DSC or rectangular temperature–time profiles. Actually, the dynamic range of commercial TMDSC apparatuses is limited and only a small part of the heat capacity spectrum can be measured by TMDSC. Nevertheless, comparison of measured base-line heat capacity with expected values from mixing rules for semi-crystalline polymers yield information about the formation (vitrification) and disappearance (devitrification) of the rigid amorphous fraction (RAF). For PC and PHB the RAF is established during isothermal crystallization while for sPP only a part of the RAF is vitrified during crystallization. Devitrification of the RAF seems to be related to the lowest endotherm.

Keywords: TMDSC; Heat capacity; Polymers; Crystallization; Rigid amorphous fraction

1. Introduction

From glass transition, it is well known and generally accepted to describe heat capacity by complex numbers. The typical frequency dependence as known from other dynamic measurements is observed—a sigmoid step in real and a peak in imaginary part of heat capacity [1–3]. Recent measurements also indicate a frequency dependence of heat capacity of semi-crystalline polymers outside the glass transition range [4,5]. These observations are related to the occurrence of an excess heat capacity that can be observed in a rather wide temperature range between glass transition and melting temperature. The origin of this excess heat capacity and its frequency dependence is not yet understood. Probably the molecular processes involved are related to the surface of the polymer crystallites and often the term reversing melting [6] is used. For polymers showing a sliding diffusion in the crystallites (α-relaxation in case of polyethylene), large contributions to reversing

* Corresponding author. Tel.: +49-381-498-1644; fax: +49-381-498-1626.
E-mail address: christoph.schick@physik.uni-rostock.de (C. Schick).

0040-6031/02/$ – see front matter
PII: S0040-6031(02)00116-8

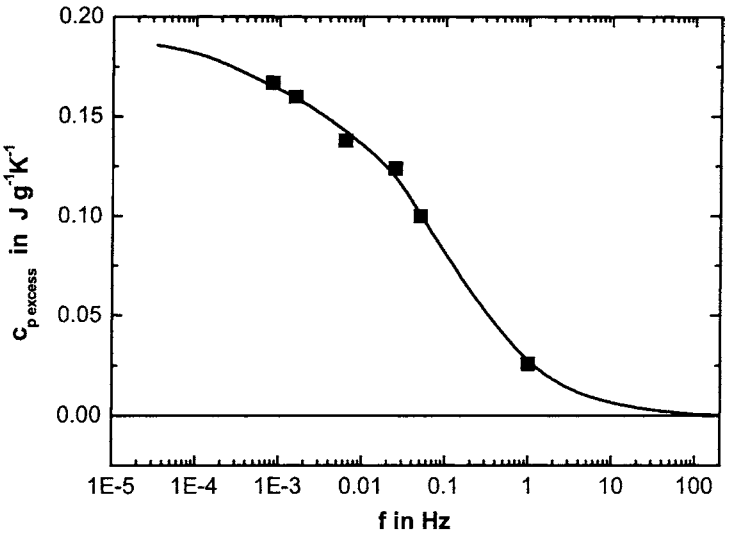

Fig. 1. Excess heat capacity of PCL after 2000 min crystallization at 328 K as a function of modulation frequency [4] (Perkin-Elmer Instruments Pyris 1 DSC and ac calorimeter [8]).

melting are due to surface melting [7]. For other semi-crystalline polymers we do not know which surfaces, growth or fold, are responsible for the process of reversing melting and the corresponding excess heat capacity.

In order to obtain information about the characteristic time scale of the molecular process related to excess heat capacity we have studied the frequency dependence of complex heat capacity during quasi-isothermal crystallization. To extend the frequency range available with temperature-modulated DSC (TMDSC) (10^{-5} to 10^{-1} Hz) ac calorimetric measurements were performed at frequency 1 Hz [8]. For polycaprolactone (PCL), a mean relaxation time in the order of seconds can be estimated for the process at 328 K. The frequency range available is still not broad enough for a detailed discussion of the curve shape, see Fig. 1. But from the curve one expects to measure base-line heat capacity without contributions due to reversing melting for frequencies higher than about 100 Hz. Base-line heat capacity corresponds to the heat necessary to increase the temperature of the sample without changing crystallinity. In other words, it is the heat capacity without any contribution from latent heats. On the other hand, at low frequencies, below 10^{-5} Hz in Fig. 1, the asymptotic value of heat capacity yields information about the total amount of material taking part in the process of reversing melting.

If base-line heat capacity is available in the temperature range between conventional glass transition and melting, it is possible to study vitrification and devitrification of the rigid amorphous fraction (RAF) of semi-crystalline polymers. There are two possible paths to reach this goal. To extend the frequency range of heat capacity measurements to the necessary high frequencies or to study polymers with very slow dynamics of the reversing melting so that the high frequency limit is reached at standard frequencies of TMDSC. For PCL, as an example, frequencies above 100 Hz are necessary to measure base-line heat capacity, see Fig. 1. This is far above the TMDSC high frequency limit of 0.1 Hz. We used the second approach and have studied bisphenol-A polycarbonate (PC) and poly(3-hydroxybutyrate) (PHB). PC was chosen for this study because of its very slow crystallization behavior [9]. Why PHB does not show reversing melting in the temperature range where it can be crystallized is not known. PHB is able to crystallize relatively fast and, for polymers, high degrees of crystallinity (0.6–0.8) can be easily reached. We compare the measured base-line heat capacities of PC and PHB with estimated heat capacities from mixing rules [10,11] to detect vitrification and devitrification of the RAF, for details, see [12]. In this paper we present frequency dependent heat capacity for semi-crystalline PC, PHB and syndiotactic polypropylene (sPP).

2. Experimental

TMDSC, a technique described for the first time in 1971 by Gobrecht et al. [1], and the necessary data treatments are described elsewhere [1,13–17]. If one wants to perform TMDSC measurements in a broad frequency range the results from high sensitive DSC apparatuses with different time constants like Perkin-Elmer Pyris 1 DSC and Setaram DSC 121 must be combined, for details, see [18]. For measurements at a fixed frequency of 0.01 Hz a TA Instruments DSC 2920 was used. For the comparison of various experimental data sets, a careful temperature calibration of all instruments is necessary. The DSCs are calibrated at zero heating rate according to the GEFTA recommendation [19]. The calibration was checked in TMDSC mode with the smectic A to nematic transition of 8OCB [20,21].

The PCL is a commercial sample from Aldrich Chemie with a molecular weight average $M_w = 55{,}700$ g/mol. More details about the sample are reported in [22]. The bisphenol-A PC was obtained from General Electric (trade name LEXAN^{TM}) and was purified by dissolution in chloroform, filtering and precipitation in methanol [23,24]. The weight average molar mass and polydispersity index for the polycarbonate were obtained by gel permeation chromatography in chloroform ($M_w = 28{,}400$ g/mol and $M_w/M_n = 2.04$). PHB was received from the University of Cairo (Prof. A. Mansour). The sPP is a commercial product from FINA Chemicals.

The heat capacity data for these polymers in the liquid and the crystalline state, except for PHB, are available from ATHAS data bank [11]. For most polymers it is not possible directly to measure heat capacity of the crystalline phase because crystallinity is limited. Fortunately, heat capacity of the glassy polymer (below glass transition) is very close to the heat capacity of the crystalline polymer. In Fig. 2 heat capacities for the amorphous (glassy) and crystalline state for the polymers under investigation are shown versus a normalized temperature scale. The data were taken from the ATHAS data bank [11] and no difference larger than the uncertainty of 3% given for the data [11] can be observed.

For PHB the corresponding heat capacities were measured for an initially amorphous sample on heating, see Fig. 3. The heat capacity for the liquid PHB was obtained from the line connecting the region above glass transition (275–300 K) with the melt (450–473 K). The straight line $c_{p\,\mathrm{liquid}}(T) = 1.1\,\mathrm{J\,g^{-1}\,K^{-1}} + 0.00208\,\mathrm{J\,g^{-1}\,K^{-2}} \times T$ is a reasonable fit for both regions and support the linear temperature dependence of c_p in the melt and super-cooled melt. The heat capacity for the solid PHB was obtained from a linear fit on the data below glass transition (220–260 K). Here we assume that the heat capacity of the solid (crystalline and glassy) polymer equals the heat capacity

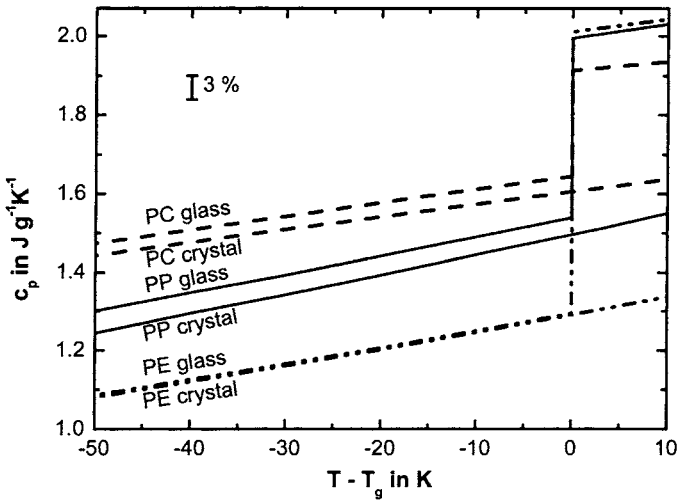

Fig. 2. Specific heat capacity for amorphous (glassy at negative and liquid at positive normalized temperatures) and crystalline PC, PP and PE as indicated. Data from [11]. The bar indicates the uncertainty of 3% for the data according to [11].

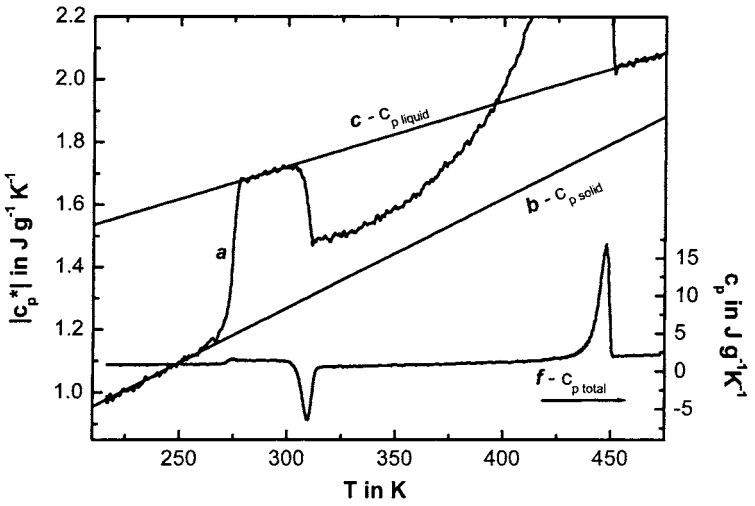

Fig. 3. TMDSC scan measurement of initially amorphous PHB at underlying heating rate 1 K min^{-1}, temperature amplitude 0.4 K and period 60 s, curve 'a'. Curves 'b' and 'c' correspond to heat capacities for solid and liquid PHB, respectively, see text. Curve 'f' shows the total heat capacity (Perkin-Elmer Instruments Pyris 1 DSC).

of the glassy polymer in the temperature interval of interest. The fit yields $c_{p\,\mathrm{solid}}(T) = 0.22\,\mathrm{J\,g^{-1}\,K^{-1}} + 0.0035\,\mathrm{J\,g^{-1}\,K^{-2}} \times T$. The same line was obtained for the semi-crystalline PHB and supports the assumption of equal heat capacities for crystalline and glassy polymers close to the glass transition temperature. This behavior seems to be general for polymers.

Because heat capacities are additive, base-line heat capacity can be obtained from mixing rules. Details of this estimation are given in [12]. In a first approximation the expected base-line heat capacity c_{pb} for the semi-crystalline sample can be calculated using a two-phase model according to

$$c_{pb}(T,t) = \chi_{\mathrm{crystal}}(T,t)c_{p\,\mathrm{crystal}}(T) + (1-\chi_{\mathrm{crystal}}(T,t))c_{p\,\mathrm{liquid}}(T) \quad (1)$$

with $c_{p\ \mathrm{crystal}}$ the specific heat capacity for the crystal which is assumed to be equal to $c_{p\ \mathrm{solid}}$, $c_{p\ \mathrm{liquid}}$ the specific heat capacity for the melt and $\chi_{\mathrm{crystal}}(T, t)$ the degree of crystallinity. For most polymers, deviations from such a simple two-phase model are observed [25,26]. Introducing a rigid amorphous fraction the base-line heat capacity can be obtained from

$$c_{pb}(T,t) = \chi_{\mathrm{solid}}(T,t)c_{p\,\mathrm{solid}}(T) + (1-\chi_{\mathrm{solid}}(T,t))c_{p\,\mathrm{liquid}}(T) \quad (2)$$

with $c_{p\ \mathrm{solid}}$ the specific heat capacity of the solid fraction $\chi_{\mathrm{solid}}(T, t)$. The solid fraction contains the crystalline and the rigid amorphous material. At the glass transition temperature $\chi_{\mathrm{solid}}(T_g)$ can be obtained from the heat capacity increment.

$$\chi_{\mathrm{solid}}(T_g) = 1 - \frac{\Delta c_p}{\Delta c_{p\,\mathrm{amorph}}} \quad (3)$$

where Δc_p is the heat capacity increment of the semi-crystalline sample while $\Delta c_{p\ \mathrm{amorph}}$ is that of the totally amorphous sample. In order to obtain $\chi_{\mathrm{solid}}(T_g)$ of the isothermally crystallized polymers the samples were cooled below T_g after crystallization and Δc_p was obtained from a TMDSC scan measurement on heating to the melt. The heat of fusion was determined from $c_{p\ \mathrm{total}}$ and $\chi_{\mathrm{crystal}}(T)$ was calculated according to the procedure suggested by Mathot [27]. In [12] we compare the expected base-line heat capacities from Eqs. (1) and (2) with measured values for PC and PHB. The values from Eq. (2) fit the measured data in a temperature range between glass transition and the first melting endotherm (annealing peak). The same is true for quasi-isothermal crystallization experiments. It was shown [12,28] that the RAF for PC and PHB is established during isothermal crystallization, see Figs. 4 and 5 and probably devitrifies at the lowest

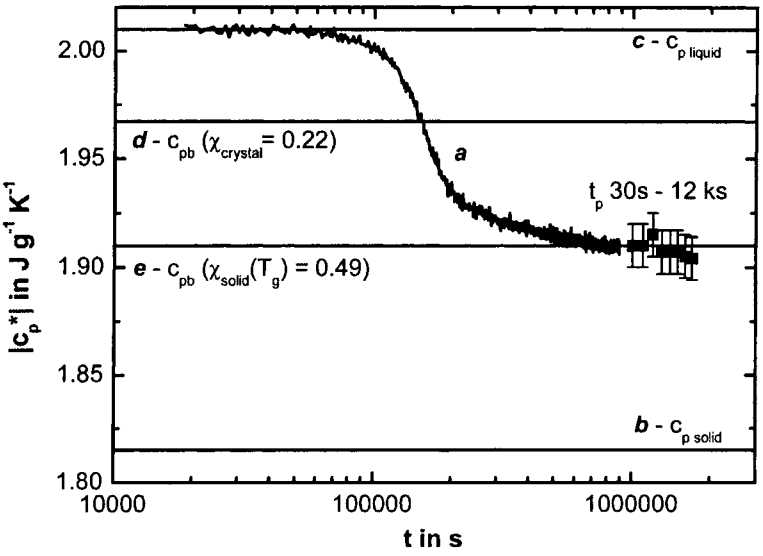

Fig. 4. Time evolution of heat capacity during quasi-isothermal crystallization of PC at 456.8 K, temperature amplitude 0.5 K and period 100 s, curve 'a'. Curves 'b' and 'c' correspond to crystalline and liquid heat capacities from ATHAS data bank, respectively. Curve 'd' was estimated from a two-phase model (Eq. (1)) and curve 'e' from a three-phase model (Eq. (2)) using $\chi_{solid}(T_g)$ from Eq. (3). The squares represent measurements at modulation periods ranging from 30 to 12,000 s (TA Instruments DSC 2920, Perkin-Elmer Instruments Pyris 1 DSC and Setaram DSC 121).

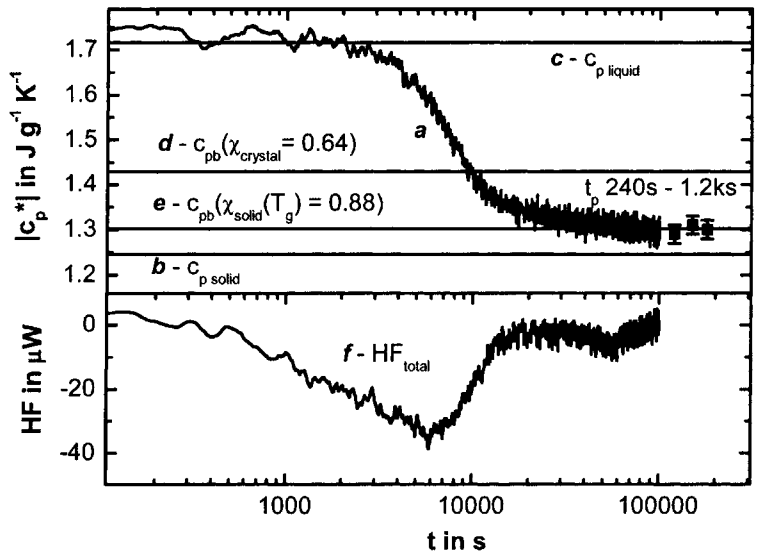

Fig. 5. Time evolution of heat capacity during quasi-isothermal crystallization of PHB at 296 K, temperature amplitude 0.4 K and period 100 s, curve 'a'. Curves 'b' and 'c' correspond to solid and liquid heat capacities, respectively. Curve 'd' was estimated from a two-phase model (Eq. (1)) and curve 'e' from a three-phase model (Eq. (2)) using $\chi_{solid}(T_g)$ from Eq. (3). The squares represent measurements at modulation periods ranging from 240 to 1200 s. Curve 'f' shows the exothermal effect in the total heat flow (Perkin-Elmer Instruments Pyris 1 DSC).

endotherm. In this paper we will extend this study to the isothermal crystallization of sPP at 363 K.

3. Results

For PC and PHB no excess heat capacity can be observed at the end of quasi-isothermal crystallization experiments, see Figs. 4 and 5 [12]. Consequently, no frequency dependence is expected.

In Figs. 4 and 5 the time evolution of heat capacity during isothermal crystallization of PC at 456.8 K and PHB at 296 K, respectively, is shown. To check whether or not base-line heat capacity is measured the frequency dependence was studied at the end of crystallization, points. No frequency dependence of measured heat capacity can be seen indicating the absence of reversing melting and that base-line heat capacity was obtained. Measured heat capacity becomes smaller than base-line heat capacity according to Eq. (1) and curve 'd', indicating the occurrence of a significant RAF during the crystallization process. On the other hand, the expected heat capacity, taking into account the RAF obtained at the glass transition, curve 'e', is in perfect agreement with the measured value at the end of isothermal crystallization. There is no difference in the amount of the RAF at crystallization and at glass transition temperature, also T_g is more than 30 K below crystallization temperature in case of PC. Therefore, we can conclude that the total RAF of PC and PHB is established (vitrified) during the isothermal crystallization. No additional vitrification occurs on cooling from the crystallization to the glass transition temperature.

In general the situation is more complicated as shown in Fig. 6 on the example of sPP. Heat capacity for sPP shows strong frequency dependence in the temperature range between glass transition and final melting on heating. This indicates the occurrence of reversing melting and the corresponding excess heat capacity.

Because changes in morphology cannot be excluded for different measurements at different frequencies the data were obtained from a single heating scan applying simultaneously a broad frequency spectrum in the perturbation. Part of the used StepScan™ temperature–time and heating rate–time profiles as well as the resulting heat flow–time response are shown in Fig. 7.

The heating steps, $q = 10\ \mathrm{K\ min^{-1}}$, yield peaks in heating rate which contain a broad spectrum of higher harmonics. In ideal case, if the peak is a delta function, all higher harmonics would have the same amplitude in heating rate. For the real system higher harmonics

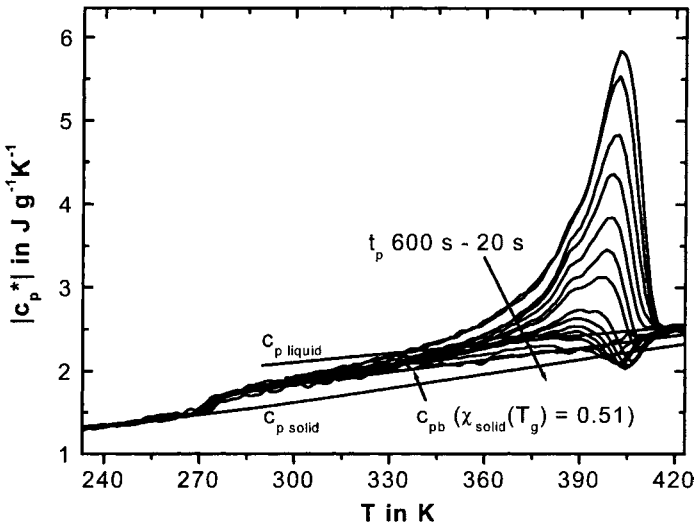

Fig. 6. Frequency dependence of specific heat capacity of sPP obtained from a single StepScan™ DSC measurement. The temperature–time profile is shown in Fig. 7 (Perkin-Elmer Instruments Pyris 1 DSC).

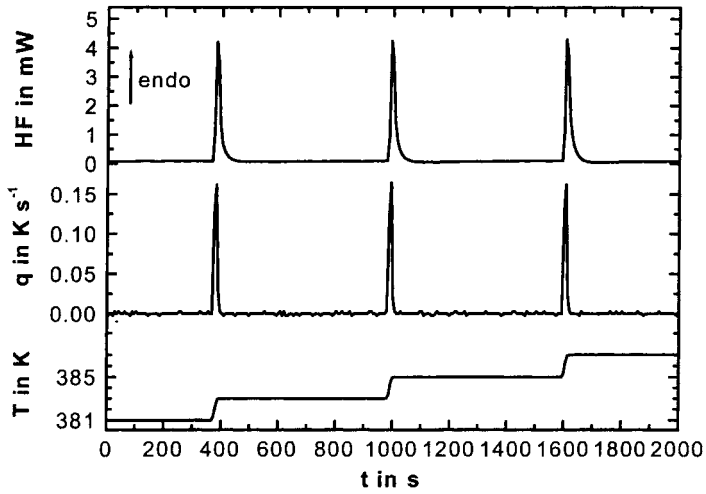

Fig. 7. Part of the measured temperature–time profile (bottom), the heating rate–time profile (middle), and the heat flow rate–time profile (top), of the StepScan™ DSC measurement from Fig. 6. The programmed step was 2 K, heating rate 10 K min^{-1} and isothermal waiting time ca. 10 min (not constant) (Perkin-Elmer Instruments Pyris 1 DSC).

are damped because of the low pass behavior of the DSC apparatus. In Fig. 8 the programmed and the measured heating rate spectra are shown.

As shown in Fig. 7 the peaks in heat flow are significantly broader than the peaks in heating rate, indicating a delayed response of the sample. From the spectra of heat flow and heating rate the spectrum of heat capacity can be obtained, for details, see [29]. The heat capacity spectra at 333 and 373 K obtained by Fourier analysis are shown in Fig. 9.

At 373 K a strong frequency dependence can be seen while at 333 K the relaxation process seems to be shifted towards lower frequencies. For both temperatures excess heat capacity probably becomes frequency independent at frequencies above 50 mHz. Therefore, one can try to check whether or not the

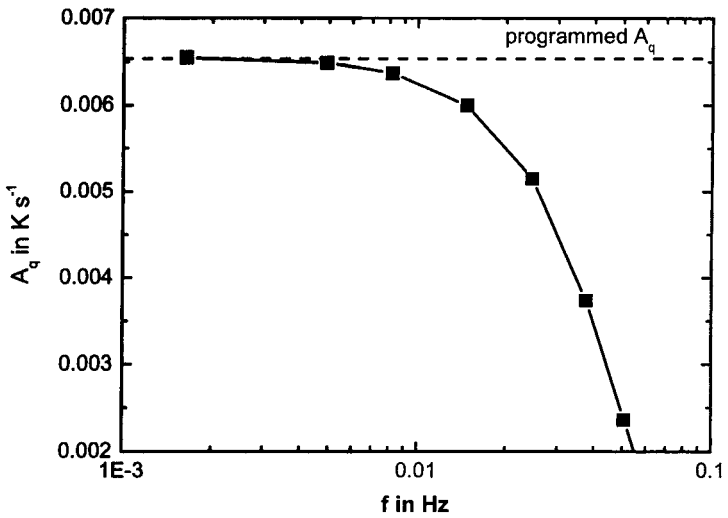

Fig. 8. Amplitude of programmed (dashed line) and measured (squares) heating rate amplitude for the data from Fig. 7.

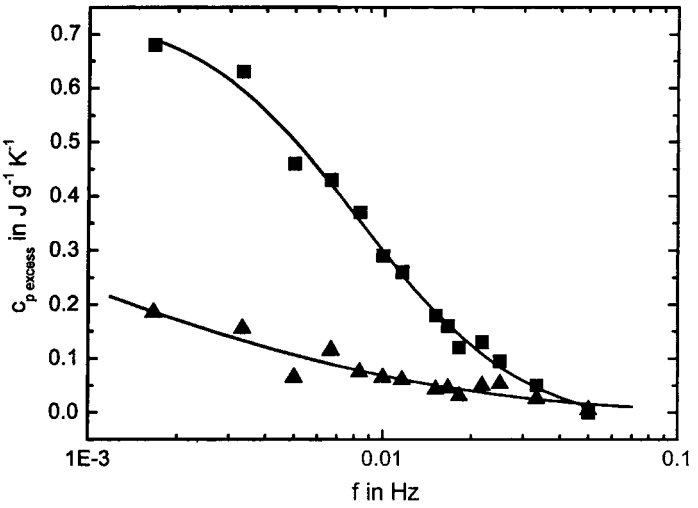

Fig. 9. Excess heat capacity for sPP on heating at 333 K (triangles), and 373 K (squares), as a function of frequency. The lines are guides for the eyes only. Data from a single StepScan^{TM} DSC measurement, for details, see Figs. 6–8.

RAF in sPP is vitrified during crystallization or not. Because sPP crystallizes fast in the temperature range between 333 and 373 K we were not able to follow crystallization by heat capacity measurements. But it is enough to measure frequency dependence of heat capacity at the end of isothermal crystallization and to compare the measured with the expected values. The result of such an experiment after crystallization at 363 K is shown in Fig. 10.

Heat capacity increases with decreasing frequency below 4 mHz. Around 0.1 mHz the measured value is larger than the heat capacity of the liquid. This is not possible without contributions from latent heat due to reversing melting. At frequencies above 10 mHz heat

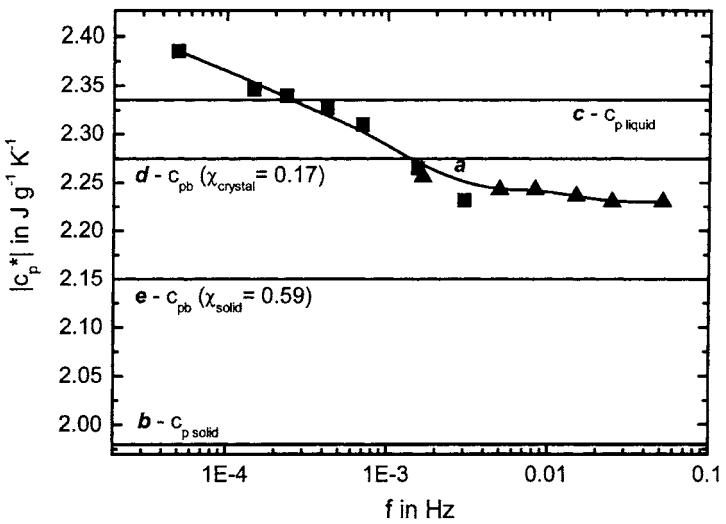

Fig. 10. Modulus of specific complex heat capacity of sPP after crystallization at 363 K for 3 h as a function of frequency. Quasi-isothermal rectangular multi-frequency temperature–time profile with period 600 s (triangles) (Perkin-Elmer Instruments Pyris 1 DSC), and 20,000 s (squares) (Setaram DSC 121). Temperature amplitude 1 K.

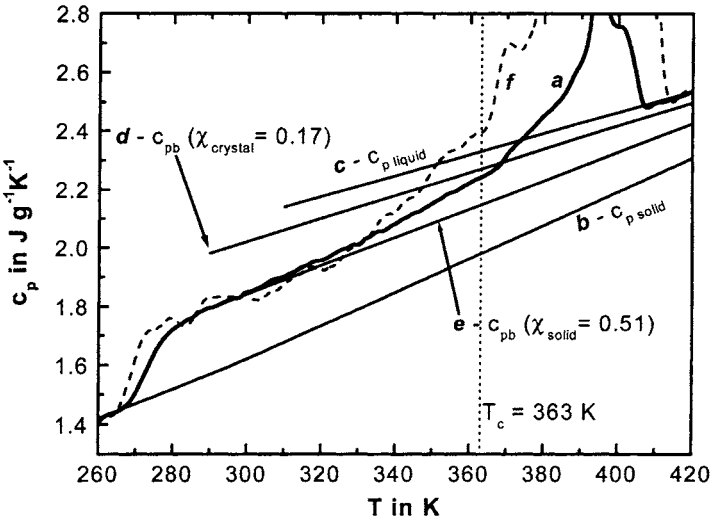

Fig. 11. TMDSC scan measurement of sPP after crystallization at 363 K for 3 h at underlying heating rate 1 K min^{-1}, temperature amplitude 0.4 K and period 60 s, curve 'a' (thick line). Curves 'b' and 'c' correspond to heat capacities for solid and liquid sPP and curves 'd' and 'e' to expected heat capacities from a two- and three-phase model, respectively. Curve 'f' (thin dashed line) shows the total heat capacity. The vertical dotted line indicates the crystallization temperature (Perkin-Elmer Instruments Pyris 1 DSC).

capacity is frequency independent. The asymptotic value at high frequencies is smaller than the expected value from a two-phase model, curve 'd', but larger than the value expected from a three-phase model, curve 'e'. For sPP only a small part of the RAF detected at T_g vitrifies during isothermal crystallization. To see when the other part of the RAF vitrifies TMDSC cooling and heating scans were performed after crystallization, see Fig. 11. The heat capacities for cooling and heating are the same within line thickness.

4. Discussion

For PC, PHB and sPP a significant rigid amorphous fraction can be determined from the step of heat capacity at the glass transition. Taking into account the crystalline, the rigid amorphous and the mobile amorphous fraction information about the phases of different molecular mobility can be obtained. For PC after 11 days crystallization at 457 K crystallinity was 0.23, rigid amorphous fraction 0.26 and mobile amorphous fraction 0.51. For PHB after crystallization at 296 K for 28 h, the values were 0.64, 0.22, 0.12 and for sPP after crystallization at 363 K for 3 h, the values were 0.17, 0.34, 0.49, respectively. While PC crystallizes extremely slow, PHB and sPP crystallizes reasonable fast.

The absence of excess heat capacities in a temperature range suitable for crystallization experiments allows us to study base-line heat capacity as a function of time for PC and PHB and to compare the measured with expected values, see Figs. 4 and 5. For PC and PHB the measured heat capacity becomes significantly smaller than base-line heat capacity expected from a two-phase model (Eq. (1)). It clearly demonstrates that for these polymers the RAF is formed during the isothermal crystallization process. Furthermore, a perfect match between the measured heat capacity at the end of crystallization and the expected base-line heat capacity from a three-phase model (Eq. (2)) can be seen. Because curve 'e' was obtained, for both polymers, from Eq. (2) using the RAF determined from the heat capacity increment at T_g, there are no indications for changes in the amount of the RAF on cooling from the crystallization temperature to the glass transition. In other words, the whole RAF, detected at T_g, was established during the quasi-isothermal crystallization for PC and PHB. From these observations we can conclude that for PC and PHB there is no broad glass transition of

the RAF somewhere in between crystallization temperature and T_g. Consequently, vitrification of the RAF results from the crystallization process itself and limits the further growth of the crystals. Vitrification of the RAF is the result of morphological changes and not due to cooling. For sPP the situation is different. As can be seen from Fig. 10 the low frequency asymptotic value of the specific heat capacity after isothermal crystallization is only a little below the expected value from a two-phase model, curve 'd' (Eq. (1)) and significantly larger than the expected value obtained from the heat capacity increment at glass transition, curve 'e' (Eqs. (2) and (3)). For sPP a significant part of the RAF detected at the glass transition is still mobile at the end of the isothermal crystallization at 363 K and vitrifies on cooling. To check this, TMDSC cooling and heating scans below crystallization temperature were performed. The same curves for complex heat capacity, as shown in Fig. 11, were obtained on cooling and heating below the crystallization temperature. Curve 'a' represents the heating scan but the cooling scan from 363 to 250 K yields the same curve within line thickness. In the temperature range between 320 K and crystallization temperature significant deviations from curve 'e', three-phase model, can be observed. Near the crystallization temperature heat capacity is close to the value expected from a two-phase model, curve 'd'. For sPP, contrary to PC and PHB, the RAF mainly vitrifies on cooling from crystallization temperature to the glass transition within ca. 40 K. Consequently, crystallization cannot be limited by the vitrification of the melt surrounding the growing crystals. For sPP other reasons must be responsible for the very low degree of crystallinity finally reached after isothermal crystallization. It may be the length distribution of crystallizable sequences of the necessary stereo regularity which limits crystallization. Why the RAF vitrifies on cooling is still an open question. There may be a temperature induced glass transition because of limited mobility of the melt. But from the total heat capacity, curve 'f', deviations from curve 'e' due to latent heats because of first melting can be observed above 330 K. This indicates crystallization of small crystals, size defined by the length of the crystallizable sequences, on cooling and melting on heating. Then vitrification of the RAF would again be the consequence of changes in morphology as for PC and PHB.

Above the crystallization temperature a small annealing peak can be seen. As for PC and PHB an increase of complex heat capacity can be seen at this peak. This indicates the devitrification of the remaining RAF as well as the occurrence of reversible melting.

5. Conclusion

For PC, PHB and sPP the asymptotic value of heat capacity at high frequencies, see Fig. 1, can be measured by TMDSC. This allows measuring base-line heat capacity and to study the formation of RAF. For PC and PHB the RAF is totally established during isothermal crystallization as can be seen from Figs. 4 and 5. Devitrification of the RAF seems to be related to the lowest endotherm as shown in [12]. The immobilization of the amorphous material around less perfect crystals, which are formed during isothermal crystallization, results in the vitrification of the RAF during crystallization and in its devitrification during melting for PC and PHB. For sPP only a small fraction of the RAF detected at the glass transition is vitrified during isothermal crystallization. These differences regarding the vitrification of the RAF indicate differences in the crystallization process. While for PC and PHB crystallization seems to be limited by the vitrification of the melt surrounding the growing crystals for sPP other mechanisms must be responsible for the low degree of crystallinity reached.

Frequency dependent heat capacity, in the high frequency limit, yield quantitative information about fractions of different mobility during the crystallization process and, how mobility of the melt is influenced by the crystallization process itself. From the step in heat capacity versus frequency information about the characteristic time scale of attachment and detachment processes of polymer segments at the crystal surface can be obtained. In order to perform such measurements the frequency range of heat capacity measurements has to be enlarged. Our results accentuates the interplay between molecular mobility of the melt and polymer crystallization [30,31]. Hopefully, a more complex view, taking into account the structure and properties of the melt surrounding the growing crystals, will help to solve some of the still open questions of polymer crystallization [32].

Acknowledgements

We are thankful to Prof. H. Marand, Blacksburg, VA, for supplying the PC sample and to Prof. A. Mansour, Cairo, for supplying the PHB sample and to both for stimulating discussions. This research was supported by the European Commission (Grant IC15CT96-0821), the German Science Foundation (Grant DFG Schi-331/5-1) (AW) and the Government of Egypt (AM). We acknowledge support by Perkin-Elmer Instruments and TA Instruments.

References

[1] H. Gobrecht, K. Hamann, G. Willers, J. Phys. E: Sci. Instrum. 4 (1971) 21.
[2] N.O. Birge, S.R. Nagel, Phys. Rev. Lett. 54 (1985) 2674.
[3] S. Weyer, A. Hensel, J. Korus, E. Donth, C. Schick, Thermochim. Acta 304/305 (1997) 251.
[4] Y. Saruyama, Thermochim. Acta 267 (1995) 75.
[5] C. Schick, M. Merzlyakov, A. Minakov, A. Wurm, J. Therm. Anal. Calc. 59 (2000) 279.
[6] I. Okazaki, B. Wunderlich, Macromolecules 30 (1997) 1758.
[7] W. Hu, T. Albrecht, G. Strobl, Macromolecules 32 (1999) 7548.
[8] A.A. Minakov, Y.V. Bugoslavsky, C. Schick, Thermochim. Acta 317 (1998) 117.
[9] S. Sohn, Crystallization behavior of bisphenol-A polycarbonate: effect of time, temperature and molar mass, Ph.D. Thesis, Virginia Polytechnic and State University, April 2000.
[10] B. Wunderlich, M. Pyda, J. Pak, R. Androsch, Thermochim. Acta 377 (2001) 9.
[11] B. Wunderlich, Pure Appl. Chem. 67 (1995) 1019, http://web.utk.edu/~athas/databank/intro.html.
[12] C. Schick, A. Wurm, A. Mohamed, Colloid Polym. Sci. 279 (2001) 800.
[13] B. Wunderlich, Y.M. Jin, A. Boller, Thermochim. Acta 238 (1994) 277.
[14] M. Reading, Trends Polym. Sci. 8 (1993) 248.
[15] J.E.K. Schawe, Thermochim. Acta 260 (1995) 1.
[16] M. Merzlyakov, C. Schick, Thermochim. Acta 330 (1999) 55, 65.
[17] S. Weyer, A. Hensel, C. Schick, Thermochim. Acta 304/305 (1997) 267.
[18] M. Merzlyakov, A. Wurm, M. Zorzut, C. Schick, J. Macromol. Sci. Phys. 38 (1999) 1045.
[19] S.M. Sarge, W. Hemminger, E. Gmelin, G.W.H. Höhne, H.K. Cammenga, W. Eysel, J. Therm. Anal. 49 (1997) 1125.
[20] A. Hensel, C. Schick, Thermochim. Acta 304/305 (1997) 229.
[21] C. Schick, U. Jonsson, T. Vassiliev, A. Minakov, J. Schawe, R. Scherrenberg, D. Lörinczy, Thermochim. Acta 347 (2000) 53.
[22] P. Skoglund, A. Fransson, J. Appl. Polym. Sci. 61 (1996) 2455.
[23] S. Sohn, A. Alizadeh, H. Marand, Polymer 41 (2000) 8879.
[24] A. Alizadeh, S. Sohn, J. Quinn, H. Marand, L. Shank, H.D. Iler, Macromolecules, 34 (2001) 4066.
[25] Y. Ishida, K. Yamafuji, H. Ito, M. Takayanagi, Kolloid-Zeitschrift and Zeitschrift für Polymere 184 (1962) 97.
[26] H. Suzuki, J. Grebowicz, B. Wunderlich, Makromol. Chem. 186 (1985) 1109.
[27] V.B.F. Mathot, Calorimetry and Thermal Analysis, Hanser, Munich, 1994 (Chapter 5.2).
[28] C. Schick, A. Wurm, M. Merzlyakov, A. Minakov, H. Marand, J. Therm. Anal. Calc. 64 (2001) 549.
[29] M. Merzlyakov, C. Schick, Thermochim. Acta 380 (2001) 5.
[30] G. Strobl, Eur. Phys. J. E 3 (2000) 165.
[31] H. Marand, A. Alizadeh, R. Farmer, R. Desai, V. Velikov, Macromolecules 33 (2000) 3392.
[32] P.H. Geil, Polymer 41 (2000) 8983.